

Ion implantation process and lattice damage mechanism of boron doped crystalline germanium

HABIBA Um E^{1,2}, CHEN Tian-Ye^{1,5}, LIU Chi-Xian^{1,5}, DOU Wei^{1,5}, LIU Xiao-Yan^{1,3}, LING Jing-Wei¹,
PAN Chang-Yi^{1,3}, WANG Peng^{1,2}, DENG Hui-Yong^{1,2,4*}, SHEN Hong^{1,2*}, DAI Ning^{1,2,3,4*}

- (1. State Key Laboratory of Infrared Physics, Shanghai Institute of Technical Physics, Chinese Academy of Sciences, Shanghai 200083, China;
2. University of Chinese Academy of Sciences, Beijing 100049, China;
3. College of Physics and Optoelectronic Engineering, Hangzhou Institute for Advanced Study, University of Chinese Academy of Sciences, Hangzhou 310024, China;
4. Zhejiang Laboratory, Hangzhou 311100, China;
5. School of Physical Science and Technology, ShanghaiTech University, Shanghai 201210, China)

Abstract: The response wavelength of the blocked-impurity-band (BIB) structured infrared detector can reach 200 μm , which is the most important very long wavelength infrared astronomical detector. The ion implantation method greatly simplifies the fabrication process of the device, but it is easy to cause lattice damage, introduce crystalline defects, and lead to the increase of the dark current of detectors. Herein, the boron-doped germanium ion implantation process was studied, and the involved lattice damage mechanism was discussed. Experimental conditions involved using 80 keV energy for boron ion implantation, with doses ranging from $1 \times 10^{13} \text{ cm}^{-2}$ to $3 \times 10^{15} \text{ cm}^{-2}$. After implantation, thermal annealing at 450 $^{\circ}\text{C}$ was implemented to optimize dopant activation and mitigate the effects of ion implantation. Various sophisticated characterization techniques, including X-ray diffraction (XRD), Raman spectroscopy, X-ray photoelectron spectroscopy (XPS), and secondary ion mass spectrometry (SIMS) were used to clarify lattice damage. At lower doses, no notable structural alterations were observed. However, as the dosage increased, specific micro distortions became apparent, which could be attributed to point defects and residual strain. The created lattice damage was recovered by thermal treatment, however, an irreversible strain induced by implantation still existed at heavily dosed samples.

Key words: boron doped germanium, ion implantation, lattice damage

晶体锗掺硼的离子注入工艺与晶格损伤机理研究

HABIBA Um E^{1,2}, 陈天业^{1,5}, 刘赤县^{1,5}, 窦伟^{1,5}, 刘晓燕^{1,3}, 凌静威¹, 潘昌翊^{1,3},
王鹏^{1,2}, 邓惠勇^{1,2,4*}, 沈宏^{1,2*}, 戴宁^{1,2,3,4*}

- (1. 中国科学院上海技术物理研究所 红外物理国家重点实验室, 上海 200083;
2. 中国科学院大学, 北京 100049;
3. 国科大杭州高等研究院 物理与光电工程学院, 浙江 杭州 310024;
4. 之江实验室, 浙江 杭州 311100;
5. 上海科技大学 物质科学与技术学院, 上海 201210)

摘要: 阻挡杂质带结构红外探测器的响应波长可达 200 μm , 是最重要的甚长波长红外天文探测器。离子注入方法简化了器件的制造过程, 但容易造成晶格损伤, 引入晶体缺陷, 并导致探测器暗电流增加。文章对掺

Received date: 2024-02-01, revised date: 2024-02-24

收稿日期: 2024-02-01, 修回日期: 2024-02-24

Foundation items: Supported by National Key R&D Program of China (2023YFA1608701), National Natural Science Foundation of China (62274168, 11933006, U2141240), and Hangzhou Leading Innovation and Entrepreneurship Team (TD2020002)

Biography: HABIBA Um E (1998-), female, Pakistan, master. Research field involves solid-state electronics. E-mail: iamumehabibalhashmi@gmail.com

*Corresponding authors: E-mail: hydeng@mail. sitp. ac. cn; hongshen@mail. sitp. ac. cn; ndai@mail. sitp. ac. cn

硼离子注入工艺进行了研究,并对晶格损伤机制进行了讨论。实验条件包括使用 80 keV 能量进行硼离子注入,剂量范围为 $1 \times 10^{13} \text{ cm}^{-2}$ 至 $3 \times 10^{15} \text{ cm}^{-2}$ 。注入后,在 450 °C 下进行热退火,以优化掺杂剂活化并减轻离子注入的影响。使用了各种表征技术,包括 X 射线衍射(XRD)、拉曼光谱、X 射线光电子能谱(XPS)和二次离子质谱(SIMS)来表征其晶格损伤。在较低剂量下,未观察到明显的结构变化。然而,随着剂量的增加,特定的微观形变变得明显,这可能是由于点缺陷和残余应变造成的。热处理可以恢复产生的晶格损伤,但在高剂量下,注入引起的不可逆应变仍然存在。

关键词: 锗掺硼;离子注入;晶格损伤

中国分类号: TN3

Introduction

In the dynamic landscape of semiconductor research, germanium has captured global attention as a promising alternative to silicon in the past two decades^[1]. Boasting distinct advantages over silicon, including enhanced electron and hole mobility along with a smaller band gap, germanium is poised to play a pivotal role in shaping the evolution of upcoming optoelectronic devices^[2-3]. Its applications extend to ionizing radiation detectors, infrared (IR) photodetectors, optical components, and temperature sensors^[4-5]. Notably, compared to silicon, germanium's reduced band gap enables efficient absorption and response to extended wavelengths of infrared radiation, establishing it as a key contributor to the advancement of sophisticated IR devices. Blocked-impurity-band (BIB) detectors, doped with arsenic (Si: As) or antimony (Si: Sb) have been utilized on the Spitzer Space Telescope and James Webb Space Telescope (JWST) for detecting wavelengths in the 5 μm to 40 μm range^[6-7]. Whereas, germanium doped with shallow impurity can be used as a BIB detector responsive to longer wavelengths, up to 200 μm ^[8]. Boron stands out as the optimal choice for introducing shallow energy levels^[9]. The most widely used technique to dope semiconductors in ion implantation is due to its good control of the dopant concentration and profile, and the isotopic purity of the implanted species^[10]. By changing the impurity concentration of ion implantation, the height of the interface barrier in the BIB detector can be adjusted, significantly reducing the dark current, which can be controlled at the order of 10^{-10} A ^[11-12]. One of the critical challenges associated with ion implantation is the inadvertent creation of damage to the crystal lattice. This damage encompasses a spectrum of defects, ranging from simple point defects like vacancies and self-interstitials to more complex structures such as small and large defect clusters, and in extreme cases, fully amorphous layers of material. These structural anomalies introduce electronic (deep) levels within the semiconductor band gap, leading to alterations in the material's electrical properties^[13]. This can further be the cause of dark currents and can affect the detector's sensitivity and detectivity. So, the study of a better understanding of lattice damage in the material is very crucial.

Contrary to silicon, there is a scarcity of comprehensive studies on lattice damage in germanium resulting from ion implantation using boron as a dopant. Until now, very few reports have been available on the study of lattice damage in germanium by boron implantation.

文献标识码: A

Suresh et al. (2001) provided noticeable insights into the diffusion behavior of boron in germanium after implantation by employing secondary ion mass spectroscopy (SIMS)^[14]. Later, Yong et al. (2005) studied the effect of high concentration on the electrical and chemical properties of boron-implanted germanium^[15]. However, a thorough exploration into the nuances of the lattice damage process resulting from implantation has yet to be undertaken. Inspired by the gap in understanding, the purpose of this research is to explore the mechanism and effects of boron implantation-induced lattice damage in germanium.

1 Experiments

The process involved implanting Boron ions into undoped germanium wafers with a <100> orientation at room temperature. The boron ions, carrying an energy of 80 keV, were implanted at six different doses ranging from $1 \times 10^{13} \text{ cm}^{-2}$ to $3 \times 10^{15} \text{ cm}^{-2}$. The incident beam was inclined at an angle of 7 degrees off the surface normal. After the initial implantation of samples, X-ray diffraction (XRD) and Raman spectroscopy were employed on the as-implanted samples to analyze the structural alterations and lattice damage.

Furthermore, the samples underwent annealing at 450 °C and subsequently examined through X-ray photoelectron spectroscopy (XPS) and SIMS in conjunction with the previously employed XRD and Raman spectroscopy techniques for a better understanding of the chemical and structural changes that happened after annealing. The results revealed that the defects induced by the implantation process were predominantly eliminated after the thermal treatment except the strain residual which still exists at high doses showcasing the irreversible damage caused by ion implantation at higher doses.

2 Results and discussions

2.1 XRD analysis

To explore and confirm the alterations in the crystal lattice resulting from boron ion implantation in germanium (Ge), X-ray diffraction (XRD) was conducted along the (100) crystallographic direction. The objective was to systematically examine the diffraction patterns across a series of samples, encompassing a spectrum of boron doses ranging from $1 \times 10^{13} \text{ cm}^{-2}$ to $3 \times 10^{15} \text{ cm}^{-2}$. Samples were examined after implantation and annealing, to study the comprehensive impact of ion implantation on the germanium crystal lattice. Figure 1 (a) shows the spectra of as-implanted samples. It was observed that, for the majority

of boron doses, there were no significant deviations in the peak positions or broadening of diffraction peaks. However, at doses of $1 \times 10^{14} \text{ cm}^{-2}$ and $5 \times 10^{14} \text{ cm}^{-2}$, a slight broadening of the peak was noted, suggesting the occurrence of lattice distortions such as point defects resulting from the implantation at these doses. Additionally, for the highest dose of $3 \times 10^{15} \text{ cm}^{-2}$, a distinct shoulder peak appeared on the left side, indicating the presence of compressive strain caused by lattice damage. This observation aligns well with findings reported by Yong in implanted Ge at a boron dose of $3 \times 10^{16} \text{ cm}^{-2}$ ^[13], confirming the evidence of lattice damage-induced strain as the implantation dose increases.

However, post-annealing has mitigated some distortions in all spectra yet the widest peaks persist for the highest boron dose, even after annealing that occurs at 450°C for 60 s. Figure 1(b) shows the result after annealing. We can clearly see that there are no additional peaks of any intensity but there is still of broadening of the peaks

exists for high doses. This peak broadening is the maximum for the highest dose of $3 \times 10^{15} \text{ cm}^{-2}$, which can be attributed to the implantation-induced irreversible strain.

2.2 Raman spectroscopy

Raman spectroscopy was implied on the implanted germanium to further analyze the structural properties of boron implanted germanium. In Fig. 2, changes in Raman peak positions and intensities were observed, reflecting alterations in the germanium lattice's vibrational modes due to boron implantation. Figure 2(a) shows the Raman spectra of the as-implanted p-type Ge samples. In observations, a distinct peak was noted around 300 cm^{-1} in the Raman spectra, which can be attributed to pristine germanium crystal^[16]. There were tiny peaks of negligible intensities were observed for some doses, indication of distortion in crystal lattice structure, similar to the findings of K. P. Jain in the Raman scattering analysis of ion-implanted silicon^[17]. Furthermore, for doses up to $1 \times 10^{15} \text{ cm}^{-2}$ and $5 \times 10^{14} \text{ cm}^{-2}$, the spectra displayed a mi-

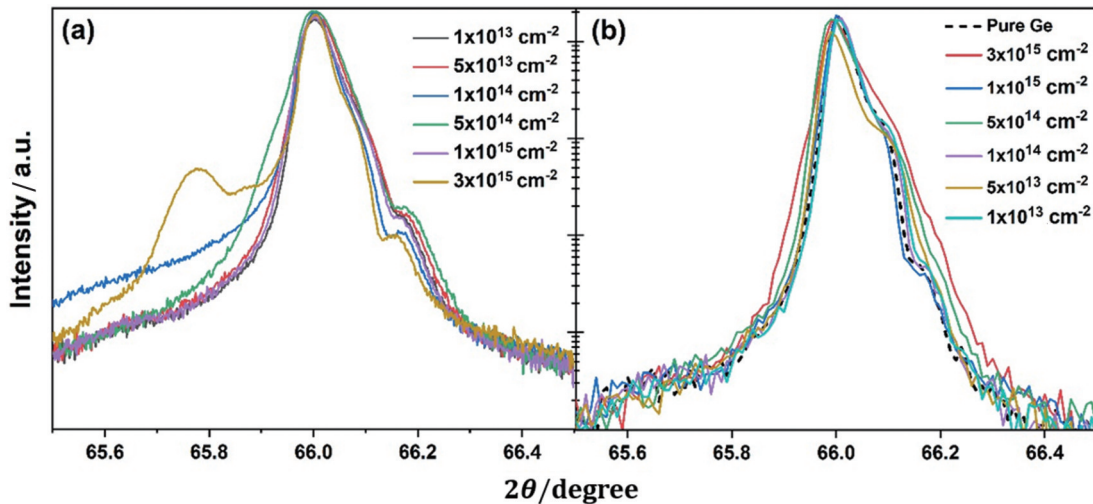


Fig. 1 XRD spectra of B implanted Ge: (a) as implanted; (b) after annealing at 450°C
图1 不同剂量B注入Ge的XRD光谱:(a)刚注入后和(b) 450°C 退火后

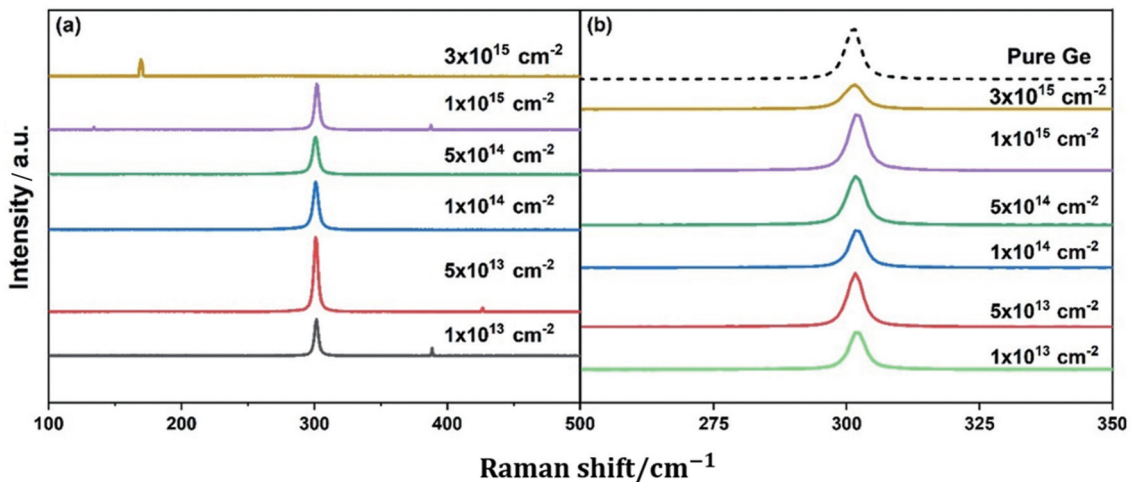


Fig. 2 Raman spectra of B implanted Ge samples at different doses: (a) as implanted; (b) annealed at 450°C
图2 不同剂量的B注入Ge样品的拉曼光谱:(a)刚注入后和(b) 450°C 退火后

nor shift of 1 cm^{-1} , $\Delta\omega = \omega_{\text{observed}} - \omega_{\text{pristine}}$.

However, a significant deviation was observed at the highest dose of $3 \times 10^{15} \text{ cm}^{-2}$ where a major Raman shift of 132 cm^{-1} was observed, as shown in Fig. 3. This deviation indicates a substantial alteration in the vibrational characteristics of the material, potentially due to strain produced by the higher dose of the implanted material. It's worth to note here that at higher doses the intensity of peaks has also decreased. This further confirms the presence of lattice strain in the sample at these higher doses, and the same trend was observed by Utamuradova in Si samples irritated by protons^[18]. The analysis shows a good agreement with XRD results. Figure 2(b) shows the Raman spectra after annealing at $450 \text{ }^\circ\text{C}$ for 60 s. The spectra reveal a distinct lack of additional peaks and discernible peak shifts. The absence of peak shifts and additional peaks in the germanium Raman spectra indicates successful restoration of the crystal lattice and minimizing ion-induced distortions. The observation of the lowest intensity for some doses even after annealing indicates that some residual effects or modifications remain in the material, persistent with the findings of XRD results.

2.3 XPS analysis

To explore the influence of implantation on elemental and chemical alterations at the sample's surface after annealing, X-ray photoelectron spectroscopy (XPS) was performed on all annealed samples. Figure 4 illustrates complete Ge^{3d} scan and C^{1s} scan of pure germanium and post-annealed boron implanted germanium samples. In the Ge^{3d} spectra of Fig. 4(a), a clear shift from pristine Ge (29.3 eV) peak^[19] is observed that shows successful introduction of boron at the sample surface.

Slight differences in peak shifts across the six samples were observed, which pointed towards potential structural changes induced by boron incorporation. Particularly, a distinctive feature emerged with a significant decrease in peak intensity for samples exposed to doses of 3×10^{15} and $5 \times 10^{14} \text{ cm}^{-2}$. This reduction in intensity even after annealing suggests presence of strain produced

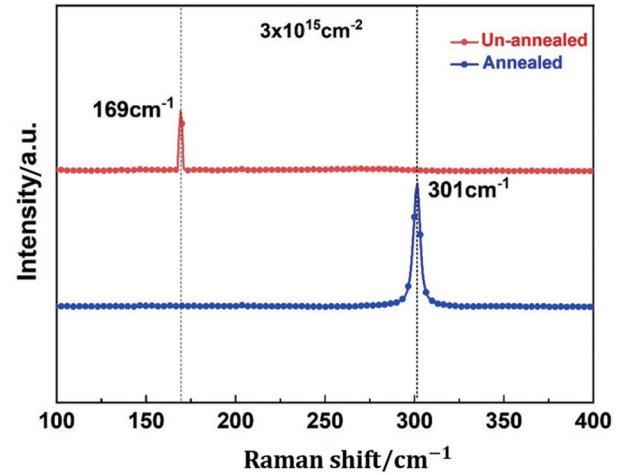


Fig. 3 Raman spectra of the germanium samples implanted at $3 \times 10^{15} \text{ cm}^{-2}$ before and after annealing

图3 $3 \times 10^{15} \text{ cm}^{-2}$ 注入剂量下, 锗样品退火前后的Raman光谱

into the lattice structure by boron incorporation. This result is consistent with the results of XRD and Raman analysis. Figure 5 illustrates the high resolution B^{1s} scan for each distinct dose. The peak analysis was performed using Gaussian fitting. The peak that consistently appears within the energy range of 181 to 184 electron volts (eV), is signifying the presence characteristic binding energy associated with boron present in the germanium lattice. The presence of satellite peaks appearing in all spectra further indicates the existence of various chemical states which lead to the formation of boron oxides within the samples, as expected in implanted materials. This is analogous to what was observed by Zhihai Cai in studying the influence of boron implantation into silicon substrate^[20]. Additionally, for B^{1s} spectra of the highest dose $3 \times 10^{15} \text{ cm}^{-2}$, there is a shift in oxidation state of boron is observed. The observed shift in oxidation state in the XPS spectra can be correlated with the lattice damage and strain induced by ion implantation at high dose. The introduction of ions into the lattice structure leads to

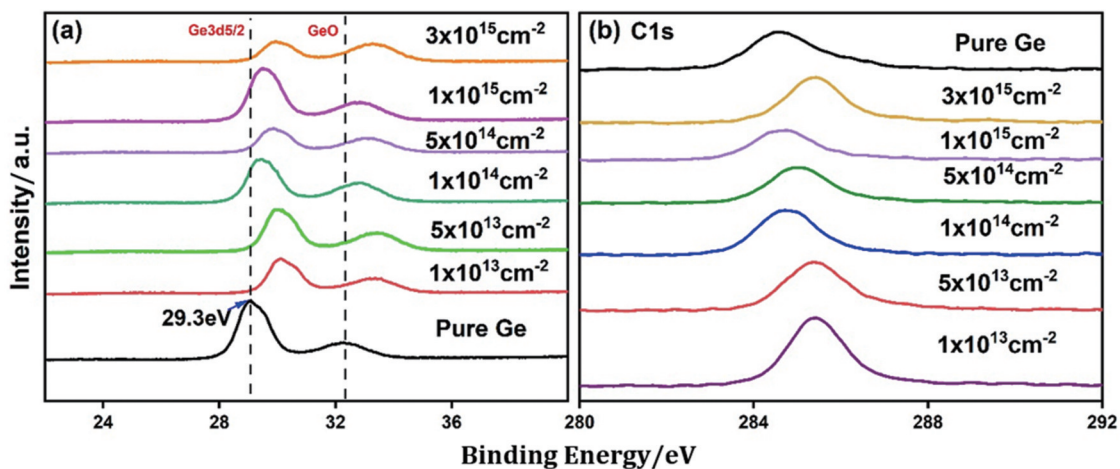


Fig. 4 XPS spectra illustrating boron implantation into germanium across distinct doses: (a) Ge^{3d} scan; (b) C^{1s} scan

图4 不同剂量下硼注入锗的XPS表征图:(a) Ge^{3d} 扫描;(b) C^{1s} 扫描

point defects and residual strain, affecting the electronic configuration of the material. This, in turn, manifests as a shift in the oxidation state, reflecting alterations in the chemical environment and bonding configurations caused by the implantation process. This further confirms our findings of XRD and Raman analysis.

2.4 SIMS depth profiling

In order to further clarify the results obtained from XRD, Raman spectroscopy, and XPS analyses, secondary ion mass spectrometry (SIMS) was employed specifically on samples subjected to two higher doses. This additional SIMS analysis aimed to provide comprehensive insights into the elemental distribution, composition, and depth profiling, enhancing our understanding of the structural and chemical modifications induced by the implantation of elevated doses which are $5 \times 10^{14} \text{ cm}^{-2}$

and $3 \times 10^{15} \text{ cm}^{-2}$. Figure 6 shows the distribution of boron within the germanium lattice, providing insights into the implantation depth and concentration. Table 1 presents key findings, highlighting relevant data on boron concentration within the germanium samples.

Notably, the projected depth R_p , as revealed by the SIMS depth profile for both doses, measures approximately $0.239 \mu\text{m}$. This uniformity in depth signifies a robust control over the implantation process, emphasizing its reproducibility. Additionally, a slight channeling tail has been observed for both doses. The observed channeling tail in this analysis aligns with the close link between the channeling effect and lattice damage in ion implantation. Channeling concentrates ion flux and induces localized strain and defects. This interplay is vital for understanding the ion penetration and distribution within the

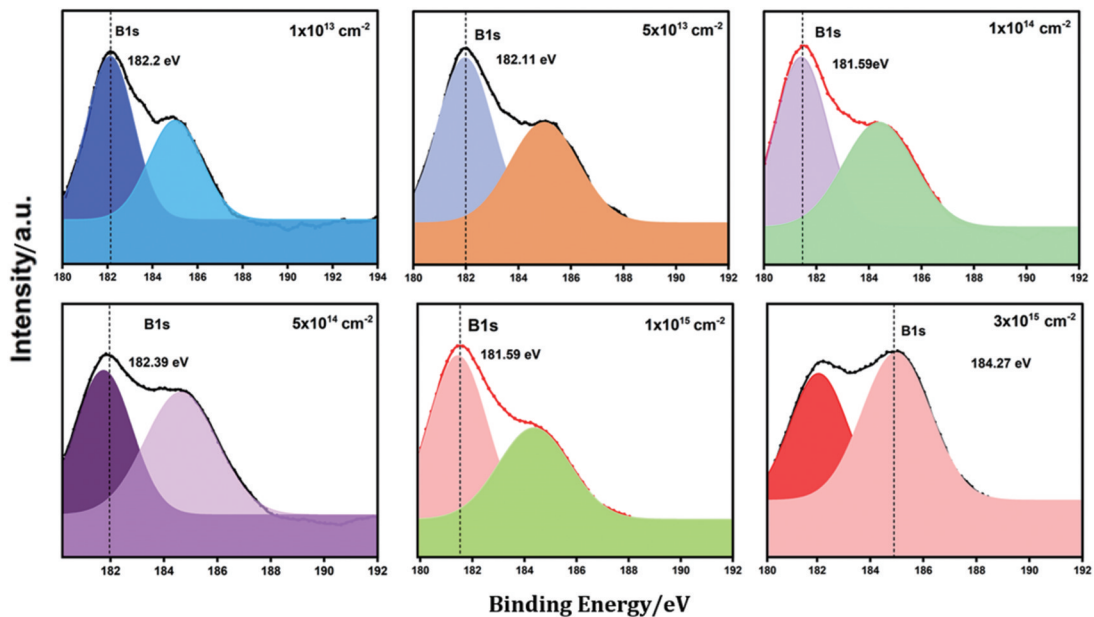


Fig. 5 XPS B^{1s} spectra illustrating boron implantation into germanium across six distinct doses
图5 六种不同剂量下硼注入锗 B^{1s} 的XPS光谱

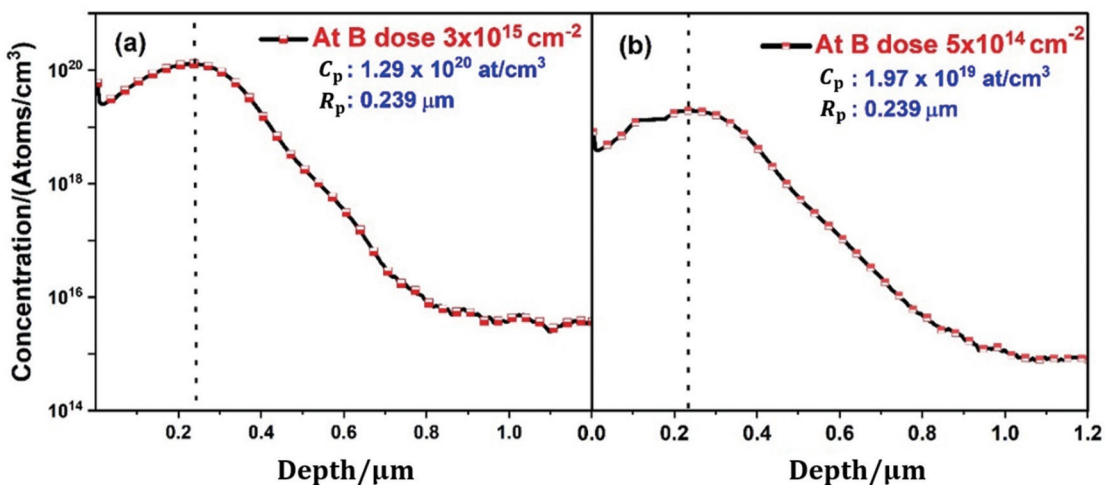


Fig. 6 SIMS analysis of B implanted Ge for two high doses: (a) $3 \times 10^{15} \text{ cm}^{-2}$; (b) $5 \times 10^{14} \text{ cm}^{-2}$
图6 两种高剂量B注入Ge的SIMS分析: (a) $3 \times 10^{15} \text{ cm}^{-2}$; (b) $5 \times 10^{14} \text{ cm}^{-2}$

Table 1 SIMS analysis results for boron implanted germanium for two specific doses
表1 两种特定剂量硼注入锗的SIMS分析结果

Dose / cm^{-2}	Concentration / (at/cm^3)	R_p / μm	Aerial Density / (at/cm^2)	Dose / (cm^{-2})	Concentration / (at/cm^3)
5×10^{14}	1.97×10^{19}	0.239	4.95×10^{14}	5×10^{14}	1.97×10^{19}
3×10^{15}	1.29×10^{20}	0.239	3.06×10^{15}	3×10^{15}	1.29×10^{20}

crystalline lattice, germanium's high stopping power further amplifies these effects. This observation is in agreement with the findings of a previous study conducted by R. Wittmann who studied depth profiles for boron implanted germanium for the energy range from 5 keV to 40 keV^[21].

3 Conclusions

Boron ion implantation effects on the lattice structure of pure germanium crystals were investigated using 80 keV energy and fluencies spanning from 1×10^{13} to $3 \times 10^{15} \text{ cm}^{-2}$. This study employed a multi-technique approach, integrating X-ray diffraction (XRD), Raman spectroscopy, X-ray photoelectron spectroscopy (XPS), and secondary ion mass spectrometry (SIMS) to comprehensively analyze the structural and chemical alterations induced by boron ion implantation at these specified doses. In all cases, minimal distortions were observed at lower doses of boron ion implantation, which went away after annealing at 450 °C for 60 s, as evidenced by the comprehensive analysis by XRD and Raman spectroscopy. However, for higher doses, the study identified presence of potential residual lattice distortion, emphasizing the challenges of mitigating irreversible distortions during implantation. Residual strain due to lattice damage at high doses was confirmed from XPS and SIMS analysis. In conclusion, this research contributes valuable insights into the lattice damage induced by boron ion implantation in germanium, emphasizing the importance of understanding and mitigating these effects for the development of high-performance semiconductor devices.

References

- [1] Moskalyk R R. Review of germanium processing worldwide [J]. *Minerals engineering*, 2004, **17**(3): 393–402.
- [2] Haller E E. Germanium: From its discovery to SiGe devices [J]. *Materials science in semiconductor processing*, 2006, **9**(4–5): 408–422.
- [3] Zhang Q, Jevasuwan W, Fukata N. Morphology and boron doping control of germanium nanowires by ex situ diffusion doping [J]. *ACS Applied Electronic Materials*, 2023, **5**(8): 4674–4681.
- [4] Baudis L, Hellmig J, Klapdor-Kleingrothaus H V, et al. High-purity germanium detector ionization pulse shapes of nuclear recoils, γ -interactions and microphonism [J]. *Nuclear Instruments and Methods in Physics Research Section A: Accelerators, Spectrometers, Detectors and Associated Equipment*, 1998, **418**(2–3): 348–354.
- [5] Zhu J, Zhu H, Xu H, et al. Impact of the structural parameters on the photoresponse of terahertz blocked-impurity-band detectors with planar structure [J]. *IEEE Transactions on Terahertz Science and Technology*, 2020, **10**(4): 358–362.
- [6] Gáspár A, Rieke G H, Guillard P, et al. The quantum efficiency and diffractive image artifacts of Si: As IBC mid-IR detector arrays at 5–10 μm : Implications for the JWST/MIRI detectors [J]. *Publications of the Astronomical Society of the Pacific*, 2020, **133**(1019): 014504.
- [7] Richards P L, McCreight C R. Infrared detectors for astrophysics [J]. *Physics Today*, 2005, **58**(2): 41–47.
- [8] Beeman J W, Goyal S, Reichertz L A, et al. Ion-implanted Ge: B far-infrared blocked-impurity-band detectors [J]. *Infrared physics & technology*, 2007, **51**(1): 60–65.
- [9] Cao L C T, Hakim L, Hsu S H. Boron doping in next-generation materials for semiconductor device [M]. *Characteristics and Applications of Boron*. IntechOpen, 2022.
- [10] Current M I. Ion implantation of advanced silicon devices: Past, present and future [J]. *Materials Science in Semiconductor Processing*, 2017, **62**: 13–22.
- [11] Pan C, Yin Z, Song Z, et al. Dark-current-blocking mechanism in BIB far-infrared detectors by interfacial barriers [J]. *IEEE Transactions on Electron Devices*, 2021, **68**(6): 2804–2809.
- [12] PAN Chang-Yi, MOU Hao, YAO Xiao-Mei, et al. High performance Ge: B blocked impurity band detector developed using near-surface processing techniques [J]. *J. Infrared MillimWaves* (潘昌翊, 牟浩, 姚晓梅, 等. 近表面加工技术制备的高性能 Ge: B 阻挡杂质带探测器 [J]. *红外与毫米波学报*), 2022, **41**(2): 389–394.
- [13] Peaker A R, Markevich V, Slotte J, et al. Understanding ion implantation defects in germanium [J]. *ECS Transactions*, 2006, **3**(2): 67.
- [14] Uppal S, Willoughby A F W, Bonar J M, et al. Diffusion of ion-implanted boron in germanium [J]. *Journal of Applied Physics*, 2001, **90**(8): 4293–4295.
- [15] Suh Y S, Carroll M S, Levy R A, et al. Implantation and activation of high concentrations of boron in germanium [J]. *IEEE transactions on electron devices*, 2005, **52**(11): 2416–2421.
- [16] Bermejo D, Cardona M. Raman scattering in pure and hydrogenated amorphous germanium and silicon [J]. *Journal of Non-Crystalline Solids*, 1979, **32**(1–3): 405–419.
- [17] Jain K P, Shukla A K, Ashokan R, et al. Raman scattering from ion-implanted silicon [J]. *Physical Review B*, 1985, **32**(10): 6688.
- [18] Utamuradova S B, Daliev S K, Stanchik A V, et al. Raman spectroscopy of silicon, doped with platinum and irradiated by protons [C]// E3S Web of conferences. EDP Sciences, 2023, **402**: 14014.
- [19] Kalimuthu V, Kumar P, Kumar M, et al. Growth mechanism and optical properties of Ge nanocrystals embedded in a GeO_x matrix [J]. *Applied Physics A*, 2018, **124**: 1–8.
- [20] Cai Z, Zhang P, Tan J. The influence of boron implantation into silicon substrate on the internal stress and adhesion strength of c-BN films [J]. *Surface and Coatings Technology*, 2007, **201**(9–11): 5039–5042.
- [21] Wittmann R, Selberherr S. A study of ion implantation into crystalline germanium [J]. *Solid-state electronics*, 2007, **51**(6): 982–988.